


Communication

A Porous π -Stacked Self-Assembly of Cup-Shaped Palladium Complex for Iodine Capture

Lin-Lin Li ^{1,2,3}, Min Huang ^{2,3,4}, Ting Chen ^{2,3,4}, Xiao-Feng Xu ^{2,3}, Zhu Zhuo ^{2,3}, Wei Wang ^{2,3}
and You-Gui Huang ^{2,3,5,*} ¹ College of Chemistry, Fuzhou University, Fuzhou 350108, China² CAS Key Laboratory of Design and Assembly of Functional Nanostructures, and Fujian Provincial Key Laboratory of Nanomaterials, Fujian Institute of Research on the Structure of Matter, Chinese Academy of Sciences, Fuzhou 350002, China³ Xiamen Institute of Rare Earth Materials, Haixi Institutes, Chinese Academy of Sciences, Xiamen 361021, China⁴ College of Chemistry and Materials Science, Fujian Normal University, Fuzhou 350002, China⁵ Fujian Science & Technology Innovation Laboratory for Optoelectronic Information of China, Fuzhou 350108, China

* Correspondence: yghuang@fjirsm.ac.cn

Abstract: Acquiring adsorbents capable of effective radioiodine capture is important for nuclear waste treatment; however, it remains a challenge to develop porous materials with high and reversible iodine capture. Herein, we report a porous self-assembly constructed by a cup-shaped Pd^{II} complex through intermolecular $\pi \cdots \pi$ interactions. This self-assembly features a cubic structure with channels along all three Cartesian coordinates, which enables it to efficiently capture iodine with an adsorption capacity of 0.60 g g⁻¹ for dissolved iodine and 1.81 g g⁻¹ for iodine vapor. Furthermore, the iodine adsorbed within the channels can be readily released upon immersing the bound solid in CH₂Cl₂, which allows the recycling of the adsorbent. This work develops a new porous molecular material promising for practical iodine adsorption.

Keywords: nuclear waste; iodine; porous; $\pi \cdots \pi$ stacking; cup-shaped



Citation: Li, L.-L.; Huang, M.; Chen, T.; Xu, X.-F.; Zhuo, Z.; Wang, W.; Huang, Y.-G. A Porous π -Stacked Self-Assembly of Cup-Shaped Palladium Complex for Iodine Capture. *Molecules* **2023**, *28*, 2881. <https://doi.org/10.3390/molecules28072881>

Academic Editor: Carlo Santoro

Received: 1 March 2023

Revised: 17 March 2023

Accepted: 18 March 2023

Published: 23 March 2023



Copyright: © 2023 by the authors. Licensee MDPI, Basel, Switzerland. This article is an open access article distributed under the terms and conditions of the Creative Commons Attribution (CC BY) license (<https://creativecommons.org/licenses/by/4.0/>).

1. Introduction

As a non-greenhouse energy source, nuclear energy is most likely to replace traditional fossil fuels [1,2]. Currently, nuclear energy is widely applied in many areas related to human life [3]. With the rapid development of the nuclear energy industry, the safe disposal of nuclear waste containing radioactive species, especially radioactive iodine, has become a significant concern [4–8]. Both ¹²⁹I and ¹³¹I, which are the main radioisotopes for iodine, are harmful to its ecological surroundings and human health. ¹²⁹I is extremely dangerous because it has a long half-life (1.57 × 10⁷ years) and can be accumulated in the human thyroid gland, causing serious diseases [6]. As for ¹³¹I, it is often combined with hydrocarbons, giving rise to harmful organic compounds such as methane iodide [9–12]. Among various possible radioactive iodine species, molecular iodine (I₂) is the main pollutant in nuclear waste disposal and the nuclear accident [13,14]. Therefore, acquiring adsorbents for effective capture of I₂ is on demand.

To date, a broad range of solid adsorbents has been found to be very promising for removing molecular iodine [15–19]. These adsorbents include zeolites [20,21], functionalized clays [22], activated carbon [23], metal/covalent–organic frameworks (MOFs and COFs) [24–33], supramolecular cages [34,35], supramolecular assemblies [36–38], etc. For example, Zheng et al. reported two amorphous MOFs exhibiting very high I₂ uptake with adsorption capacities of 2.05 and 5.04 g g⁻¹ [39], respectively. Chi et al. reported that nonporous adaptive crystals of a bipyridine cage can reversibly capture I₂ [40]. In spite

of that significant progress on adsorbents for I₂ capture has been achieved, there is still much room to improve the performance of adsorbents for I₂ capture. In general, a high-performance I₂ capture material needs to simultaneously meet the following requirements: high I₂ adsorption capacity and kinetics under industrial conditions, high selectivity, a long retention time of the adsorbed I₂, and great recyclability and low-cost [14]. The search for high-performance I₂ capture adsorbents is still ongoing.

Recently, macrocycle-based supramolecular assemblies have emerged as a class of adsorbents for I₂ capture [37,41,42]. For example, Huang's group reported perethylated pillar [6] arene, which acts as a candidate for I₂ capture [41], while Zhang and co-workers directly observed the ambiguous binding sites for I₂ in a mesoporous assembly of aluminum molecular rings [42]. Recently, we have successfully obtained a series of π -stacked porous assemblies based on metal complexes of tripodal tris(2-benzimidazolylmethyl) amine or tris(2-naphthimidazolylmethyl) amine [43,44]. These achievements promoted us to synthesize porous assemblies based on metal complexes of tripodal ligands to explore high-performance adsorbents for I₂ capture.

In this work, we report a porous π -stacked self-assembly based on a cup-shaped Pd^{II} complex. Due to the channels in the structure, this material permits the capture of both dissolved I₂ and I₂ vapor. Furthermore, the present adsorbent can be reused several times without significant loss of I₂ uptake capacity.

2. Results and Discussion

2.1. Structure Characterizations of the π -Stacked Self-Assembly

The self-assembly of (2,2'-bipyridine) dichloropalladium (II)([Pd(bipy)]Cl₂) with tris(2-naphthimidazolylmethyl) amine (H₃L) in a mixture of MeOH/acetone (*v/v*: 1/3) with a trace of triethylamine affords yellow crystals of [Pd₃(bipy)₃L] Cl₃·solvent (**1**). Single-crystal X-ray analysis (Table S1) reveals a cup-shaped trinuclear Pd^{II} complex in which three [Pd(bipy)]²⁺ cations are bridged by the naphthimidazolyl arms of L, giving rise to a macrocycle (Figure 1a). Driven by the coordination mentioned above, L is fixed into an unusual cup-shaped conformation [39,40] and the three [Pd(bipy)]²⁺ cations act as the cup holder. In the crystal structure, each [Pd₃(bipy)₃L]³⁺ associates with its six neighbors (Figure 1b) through $\pi\cdots\pi$ interactions between bipy and L, forming a porous non-symmetric cubic supramolecular assembly (Figure 1c). This porous structure possesses two kinds of channels along all three crystallographic axes, which are filled with Cl⁻ and solvent molecules. Determined by PLATON, the void volume is 8658 Å³ per unit cell, which is 48.3% of the unit volume. In the view of topology, treating [Pd₃(bipy)₃L]³⁺ as a node and the $\pi\cdots\pi$ interaction between bipy and L as a linker (Figure S1a), the porous assembly can be simplified as a pcu network with a Schläfli symbol of 4⁶·6⁹ (Figure S1b). Thermogravimetric (TG) analysis with the sample heated under an N₂ stream revealed a weight loss of ~15% between 30 and 200 °C, which can be attributed to the removal of solvent molecules (Figure 2a). After desolvation, the framework structure of the porous assembly collapses, as indicated by powder X-ray diffraction (PXRD) studies (Figure 2b).

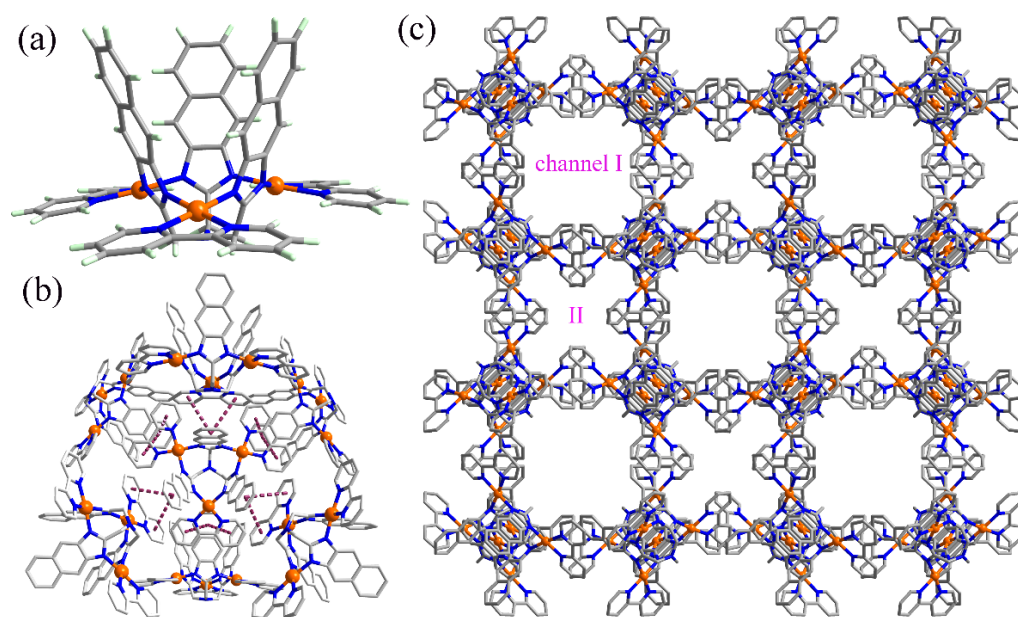


Figure 1. (a) The cup-shaped trinuclear $[\text{Pd}_3(\text{bipy})_3\text{L}]^{3+}$ in a macrocycle. Atom color codes: Pd, orange; N, blue; C, gray; H, bright white. (b) View of each macrocycle associating with its six neighbors through $\pi\cdots\pi$ interactions. (c) The porous cubic supramolecular assembly showing two types of channels.

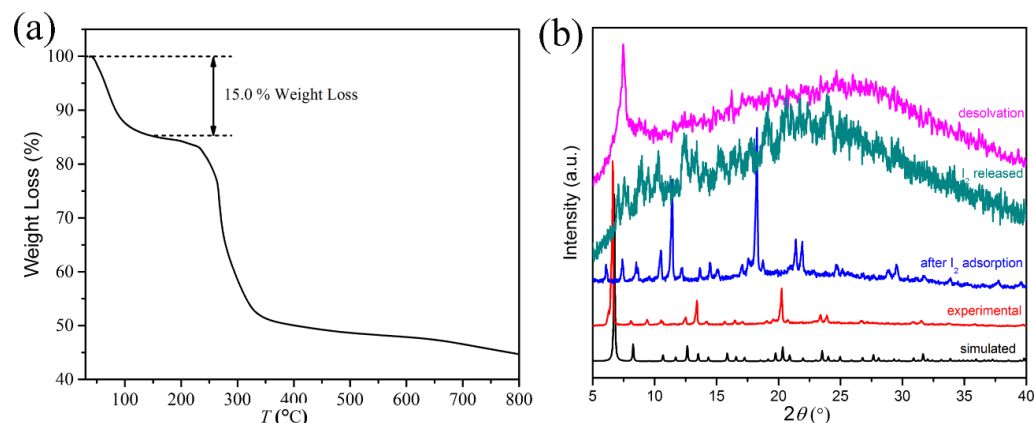


Figure 2. (a) TG analysis of compound **1**. (b) PXRD patterns of compound **1**.

2.2. Iodine Adsorption Study

The poor thermostability of compound **1** prohibits us from investigating its iodine adsorption performance at high temperatures. Therefore, the adsorption performances of compound **1** on both gaseous and dissolved iodine were investigated at room temperature. Exposing compound **1** to iodine vapor at room temperature led to a gradual color change from yellow to black (Figure S2a). The iodine uptake also gradually increased with time and attained an uptake of 1.37 g g^{-1} after 240 h without saturation (Figure 3a). The gaseous iodine adsorption profile can be well described by the pseudo-first-order kinetic model ($R^2 = 0.996$), which gives an adsorption rate $k = 1.0 \times 10^{-4} \text{ g min}^{-1}$ and an equilibrium adsorption capacity $Q_e = 1.81 \text{ g g}^{-1}$ (Table S2).

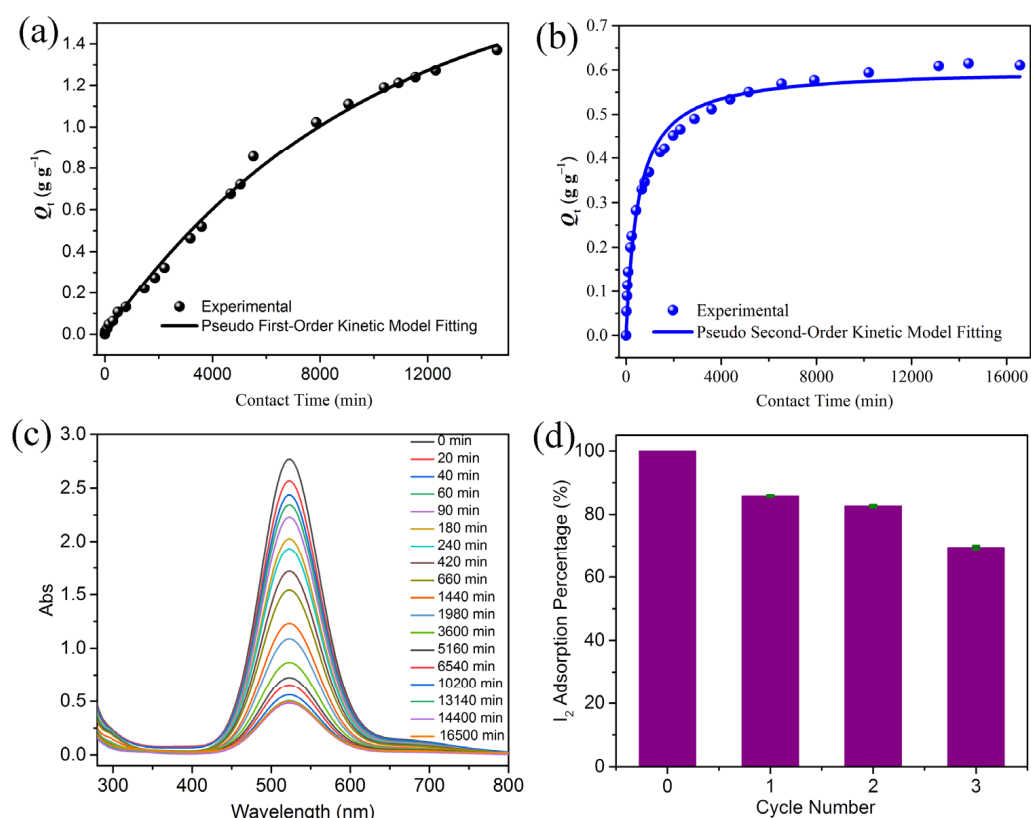


Figure 3. (a) Time-dependent iodine vapor uptake plot for the crystals of compound **1** at room temperature. (b) Time-dependent dissolved iodine uptake plot for the crystals of compound **1** at room temperature. (c) Time-dependent UV-Vis spectrum evolution of the solution of I_2 in cyclohexane with the crystals of compound **1** as adsorbent. (d) Graph showing the recyclability of compound **1** for dissolved iodine adsorption.

We then examined the adsorption performance of compound **1** for iodine dissolved in cyclohexane. A crystalline sample of compound **1** (0.05 g) was immersed in a 3 mM iodine–cyclohexane solution. UV-Vis spectroscopy was used to evaluate the iodine adsorption rate (Figures 3b,c and S3). With the adsorption going on, the color of the iodine–cyclohexane solution gradually faded (Figure S2b). The color of the sample of compound **1** gradually deepened and turned black when the adsorption equilibrium was reached (Figure S2c). The monitoring data revealed a fast adsorption rate in the first 6 h, and then the adsorption gradually slowed down until equilibrium (Figure 3b). The experimental data can be well described by the pseudo-second-order kinetic model ($R^2 = 0.977$), which gives an adsorption rate $k_2 = 3.0 \times 10^{-3} \text{ g min}^{-1}$ and an equilibrium adsorption capacity of 0.60 g g^{-1} (Figure 3b, Table S2). The gaseous I_2 and dissolved I_2 uptake capacities of compound **1** are comparable to those of some promising I_2 adsorbents (Table S3) [45–48]. Furthermore, the adsorbed iodine can be released from $I_2@1$ by soaking $I_2@1$ in CH_2Cl_2 . When 0.50 g of solid $I_2@1$ was immersed in CH_2Cl_2 , the solution gradually changed from colorless to dark brown in 36 h, indicating a large amount of I_2 was released (Figure S4). Therefore, this adsorbent for iodine capture can be recycled. In the third adsorption–desorption cycle, ~70% of the I_2 adsorption capability can be retained (Figure 3d).

To give insights into the I_2 adsorption mechanism, we conducted Fourier transform infrared (FT-IR) spectroscopy (Figure 4a) and X-ray photoelectron spectroscopy (XPS) (Figure 4b–d) studies on compound **1** before and after I_2 uptake. After I_2 loading, the characteristic band at $\sim 1634 \text{ cm}^{-1}$ assigned to the C=N stretching vibration decreases significantly [14,19,29,33,34]. A pair of I 3d signals can be seen from the XPS of the sample after I_2 uptake (Figure 4a,b). The signals at 617.84 and 629.37 eV can be attributed to $I 3d_{5/2}$ and I

$3d_{3/2}$, respectively. After I_2 loading, the two N 1s signals shift from 397.94 and 399.14 eV to 398.29 and 399.43 eV, respectively (Figure 4c). The two Pd 3d signals also shift from 336.31 and 341.51 eV to 337.88 and 343.78 eV, respectively (Figure 4d). These results indicate that the N and Pd atoms on compound **1** interact with the captured iodine [49]. This interaction may be rationalized in terms of that polarized bound iodine molecules favor interaction with the partly negatively charged N lone pairs, while the cylindrical electron surface of the I–I bond would favor interaction with the positively charged Pd atoms [45]. The PXRD of $I_2@1$ is significantly different from that of compound **1**, indicating a possible significant structural change upon iodine adsorption. However, the poor crystallinity of $I_2@1$ prohibits us from directly observing the I_2 binding sites by single-crystal X-ray analysis. The recycled sample of compound **1** that lost crystallinity probably implies good dispersion of the adsorbed iodine molecules around the cup-shaped molecules (Figure 2b).

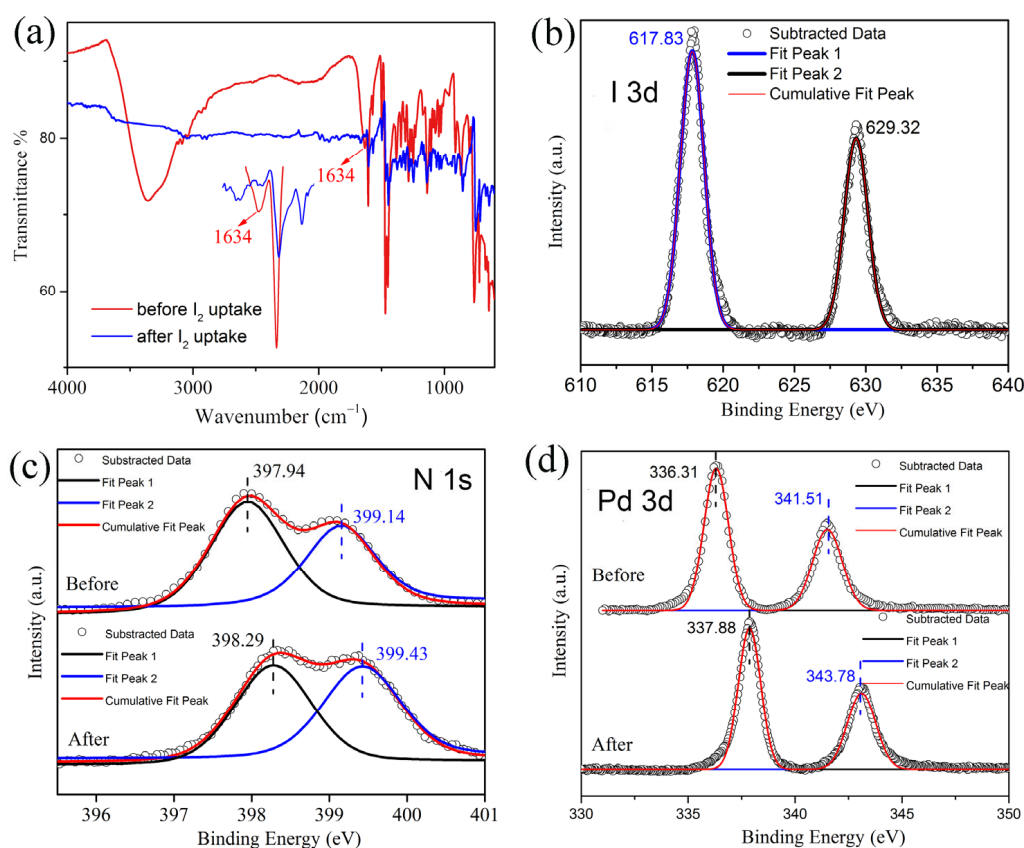


Figure 4. (a) IR spectra of compound **1** before and after I_2 uptake (inset: enlarged spectra showing the significant decrease of band at $\sim 1640\text{ cm}^{-1}$). (b) XPS of I 3d for $I_2@1$. (c) XPS of N 1s for compound **1** before and after dissolved I_2 uptake. (d) XPS of Pd 3d for compound **1** before and after dissolved I_2 uptake.

3. Experimental

3.1. Iodine Adsorption Study

The ligand H_3L is synthesized according to the previously reported method [50]. $[Pd(bipy)]Cl_2$ and 2,3-diaminonaphthalene were purchased from bidepharmatech. All other reagents were purchased from Adamas (Shanghai, China) and used directly, without purification.

3.2. Characterization

Fourier-transform infrared (FTIR, Nicolet iS 50, Thermo Fisher, Waltham, MA, USA) spectra were recorded on a Thermo Fisher Nicolet iS 50 in the range $500\text{--}4000\text{ cm}^{-1}$ at room temperature. Powder X-ray diffraction (PXRD, Miniflex 600, Akishima, Rigaku, Tokyo,

Japan) patterns were obtained on a Miniflex 600 diffractometer using Cu-K α radiation with flat plate geometry. X-ray photoelectron spectroscopy (XPS, Thermo Scientific K-Alpha, Waltham, MA, USA) studies were performed on an AXIS SUPRA Kratos system, and the C 1s line at 284.8 eV was used as the binding energy reference. TGA was performed using a thermo plus EVO2 system at a rate of 10 °C/min in the range of 30–800 °C (TGA/DSC 1, Mettler Toledo, Zurich, Switzerland). UV–Vis spectra were recorded on an Agilent Cary 5000 spectrophotometer (UV-Vis, Agilent, Santa Clara, CA, USA).

3.3. Crystallography

Single-crystal X-ray data were harvested on a Bruker D8 Venture diffractometer with Mo-K α radiation at 200 K. Structures were solved using a direct method and refined by the full-matrix least-squares technique on F2 with the SHELXTL 2014 program [51]. All the H atoms are geometrically generated and refined using a riding model. The PLATON/SQUEEZE procedures [52] were used to treat the highly disordered solvents in the void of the porous structure. The X-ray crystallographic coordinates for structures reported in this article have been deposited at the Cambridge Crystallographic Data Centre (CCDC), under deposition number CCDC 2245193. The data can be obtained free of charge from the Cambridge Crystallographic Data Centre via www.ccdc.cam.ac.uk/data_request/cif (accessed on 28 February 2023). Details of the crystallographic data are listed in Table S1.

3.4. Synthesis of Compound 1

Additionally, (2,2'-bipyridine) dichloropalladium (II) (0.030 g, 0.09 mmol), tris (2-naphthimidazole methyl) amine (H₃L) (0.020 g, 0.036 mmol), and triethylamine (0.02 mL) were added to a mixture of MeOH/acetone (*v/v*: 1/3), and the mixture was stirred at room temperature for 2 h. After that, the insoluble substance was removed through filtration. The resulting filtrate was kept at room temperature undisturbed for 7 days, and then pale green crystals were obtained (yield: 67.7% based on L).

3.5. Iodine Adsorption Experiments

Both the gaseous iodine and dissolved iodine uptake behaviors of compound 1 were studied at room temperature.

3.5.1. Iodine Vapor Adsorption

Air-dried compound 1 (0.050 g) was loaded into an uncapped glass vial, which was located in a sealed container with excess solid iodine kept at the bottom. After certain time intervals, the vial was taken out and weighed, and then reloaded into the vapor of iodine to continue adsorption. The iodine uptake at a certain time was calculated using Equation (1):

$$Q_t = \frac{m_2 - m_1}{m_1} \quad (1)$$

where Q_t represents the iodine uptake at a certain time and m_1 and m_2 are the masses of the sample of compound 1 before and after iodine uptake, respectively. The pseudo-first-order model (Equation (2)) was used to fit the gaseous iodine adsorption profile, giving a set of parameters with $k_1 = 1.0 \times 10^{-4} \text{ g min}^{-1}$, $Q_e = 1.81 \text{ g g}^{-1}$, and $R^2 = 0.996$.

$$Q_t = Q_e \left(1 - e^{-k_1 t}\right) \quad (2)$$

3.5.2. Iodine Adsorption in Solution

Air-dried compound 1 (0.050 g) was immersed in a 50 mL solution of iodine in cyclohexane (3 mM). The iodine adsorption process was monitored by UV–Vis spectroscopy. The iodine uptake was calculated using Equation (3):

$$Q_t = \frac{(C_0 - C_t)}{m} V \quad (3)$$

where Q_t represents the iodine uptake at a certain time, C_0 and C_t represent the concentration of iodine before and after adsorption, respectively, m represents the mass of compound **1**, and V represents the volume of the solution. The pseudo-second-order model (Equation (4)) was used to fit the dissolved iodine adsorption profile, giving a set of parameters with $k_2 = 3.0 \times 10^{-3} \text{ g min}^{-1}$, $Q_e = 0.60 \text{ g g}^{-1}$, and $R^2 = 0.977$.

$$Q_t = \frac{k_2 Q_e^2 t}{1 + k_2 Q_e t} \quad (4)$$

3.5.3. Iodine Release and Recyclability of Compound **1**

I₂@1 was immersed in CH_2Cl_2 to release the adsorbed iodine. Here, **I₂@1** (0.050 g) was immersed in CH_2Cl_2 (100 mL). When the release was deemed essentially complete, the resulting solid was recycled and analyzed by PXRD. Then the recycled solid of compound **1** was added to the I_2 /cyclohexane solution again. After four cycles, ~70% of the I_2 adsorption capability can be retained.

4. Conclusions

In summary, we have developed a porous self-assembly of a cup-shaped Pd^{II} complex. This porous structure is constructed through intermolecular $\pi \cdots \pi$ interactions. The channels along all three crystallographic axes within the self-assembly allow for efficient reversible iodine capture, either from the vapor or solution source phases. These results demonstrate that porous crystalline materials assembled through weak intermolecular interactions can serve as a new type of promising adsorbent for I_2 capture.

Supplementary Materials: The following supporting information can be downloaded at: <https://www.mdpi.com/article/10.3390/molecules28072881/s1>, Figure S1: (a) The simplification of the network of compound **1**, (b) The simplified pcu network of the supramolecular framework of compound **1**; Table S1: Crystallographic data of compound **1**; Figure S2: (a) The setup for I_2 vapor adsorption, (b) Photographs showing color changes of the I_2 /cyclohexane solution as a function of time when 0.050 g of compound **1** was immersed in the solution, (c) Photographs showing the color change of the crystals of compound **1** before and after dissolved I_2 adsorption, (d) Photographs showing the release of I_2 from **I₂@1** in CH_2Cl_2 ; Table S2: Fitting the iodine adsorption kinetics of compound **1**; Figure S3: Standard plot between absorbance ($\lambda = 523 \text{ nm}$) and I_2 concentration of the solution of I_2 in cyclohexane; Table S3: The comparison of I_2 adsorption capacities for various adsorbents.

Author Contributions: L.-L.L. performed experiments and wrote the paper. M.H. and T.C. collected data. X.-F.X. directed the compound characterization and data analysis. Z.Z. and W.W. contributed on interpreting the data. Y.-G.H. conceived the project. All authors have read and agreed to the published version of the manuscript.

Funding: This research was funded by the National Natural Science Found (NNSF) of China (92261109 and 21901242), the NSF of Fujian Province (2020J05080), the NSF of Xiamen (3502Z20206080), the Fujian Science and Technology Innovation Laboratory for Optoelectronic Information of China (2021ZR110), the Recruitment Program of Global Youth Experts, and the Youth Innovation Promotion Association.

Institutional Review Board Statement: Not applicable.

Informed Consent Statement: Not applicable.

Data Availability Statement: All data related to this study are presented in this publication.

Conflicts of Interest: The authors declare no conflict of interest.

Sample Availability: Samples are available from the author.

References

1. Xie, W.; Cui, D.; Zhang, S.-R.; Xu, Y.-H.; Jiang, D.-L. Iodine capture in porous organic polymers and metal-organic frameworks materials. *Mater. Horiz.* **2019**, *6*, 1571–1595. [[CrossRef](#)]
2. Ewing, R.C.; Hippel, F.N.V. Nuclear waste management in the United States-starting over. *Science* **2009**, *325*, 151–152. [[CrossRef](#)]

3. Sen, A.; Sharma, S.; Dutta, S.; Shirolkar, M.M.; Dam, G.K.; Let, S.; Ghosh, S.K. Functionalized ionic porous organic polymers exhibiting high iodine uptake from both the vapor and aqueous medium. *ACS Appl. Mater. Interfaces* **2021**, *13*, 34188–34196. [[CrossRef](#)]
4. Yan, Z.J.; Qiao, Y.M.; Wang, J.L.; Xie, J.L.; Cui, B.; Fu, Y.; Lu, J.W.; Yang, Y.J.; Bu, N.S.; Yuan, Y.; et al. An azo-group-functionalized porous aromatic framework for achieving highly efficient capture of iodine. *Molecules* **2022**, *27*, 6297. [[CrossRef](#)]
5. Kintisch, E. Congress tells DOE to take fresh look at recycling spent reactor fuel. *Science* **2005**, *310*, 1406. [[CrossRef](#)]
6. Ogilvy-Stuart, A.L.; Shalet, S.M. Effect of radiation on the human reproductive system. *Environ. Health Perspect.* **1993**, *101*, 109–116.
7. Chen, P.; He, X.H.; Pang, M.B.; Dong, X.T.; Zhao, S.; Zhang, W. Iodine capture using Zr-based metal–organic frameworks (Zr-MOFs): Adsorption performance and mechanism. *ACS Appl. Mater. Interfaces* **2020**, *12*, 20429–20439. [[CrossRef](#)]
8. Gao, R.; An, B.H.; Zhou, C.; Zhang, X. Synthesis of a triaisotruene-based porous organic polymer and its application in iodine capture. *Molecules* **2022**, *27*, 8722. [[CrossRef](#)]
9. Shimamoto, Y.S.; Takahashi, Y.; Terada, Y. Formation of organic iodine supplied as iodide in a soil-water system in Chiba, Japan. *Environ. Sci. Technol.* **2011**, *45*, 2086–2092. [[CrossRef](#)]
10. Sabri, M.A.; Al-Sayah, M.H.; Sen, S.; Ibrahim, T.H.; El-Kadri, O.M. Fluorescent aminal linked porous organic polymer for reversible iodine capture and sensing. *Sci. Rep.* **2020**, *10*, 15943. [[CrossRef](#)]
11. Ten Hoeve, J.E.; Jacobson, M.Z. Worldwide health effects of the Fukushima Daiichi nuclear accident. *Energy Environ. Sci.* **2012**, *5*, 8743–8757. [[CrossRef](#)]
12. Taylor, D.M. The radiotoxicology of iodine. *J. Radioanal. Chem.* **1981**, *65*, 195–208. [[CrossRef](#)]
13. Yamaguchi, N.; Nakano, M.; Takamatsu, R.; Tanida, H. Inorganic iodine incorporation into soil organic matter: Evidence from iodine K-edge X-ray absorption near-edge structure. *J. Environ. Radioact.* **2010**, *101*, 451–457. [[CrossRef](#)]
14. Yang, Y.T.; Tu, C.Z.; Yin, H.J.; Liu, J.J.; Cheng, F.X.; Luo, F. Molecular iodine capture by covalent organic frameworks. *Molecules* **2022**, *27*, 9045. [[CrossRef](#)]
15. Yu, C.-X.; Li, X.-J.; Zong, J.-S.; You, D.-J.; Liang, A.-P.; Zhou, Y.-L.; Li, X.-Q.; Liu, L.-L. Fabrication of protonated two-dimensional metal–organic framework nanosheets for highly efficient iodine capture from water. *Inorg. Chem.* **2022**, *61*, 13883–13892. [[CrossRef](#)]
16. Zhang, X.R.; Maddock, J.; Nenoff, T.M.; Denecke, M.A.; Yang, S.; Schröder, M. Adsorption of iodine in metal–organic framework materials. *Chem. Soc. Rev.* **2022**, *51*, 3243–3262. [[CrossRef](#)]
17. Yan, Z.J.; Cui, B.; Zhao, T.; Luo, Y.F.; Zhang, H.C.; Xie, J.L.; Li, N.; Bu, N.S.; Yuan, Y.; Xia, L.X. A carbazole-functionalized porous aromatic framework for enhancing volatile iodine capture via Lewis electron pairing. *Molecules* **2021**, *26*, 5263. [[CrossRef](#)]
18. Guan, H.; Zou, D.L.; Yu, H.Y.; Liu, M.J.; Liu, Z.; Sun, W.T.; Xu, F.F.; Li, Y.X. Adsorption behavior of iodine by novel covalent organic polymers constructed through heterostructural mixed linkers. *Front. Mater.* **2019**, *6*, 12. [[CrossRef](#)]
19. Tian, P.; Ai, Z.T.; Hu, H.; Wang, M.; Li, Y.L.; Gao, X.P.; Qian, J.Y.; Su, X.F.; Xiao, S.T.; Xu, H.J.; et al. Synthesis of electron-rich porous organic polymers via Schiff-base chemistry for efficient iodine capture. *Molecules* **2022**, *27*, 5161. [[CrossRef](#)]
20. Pham, T.C.T.; Docao, S.; Hwang, I.C.; Song, M.K.; Choi, D.Y.; Moon, D.; Oleynikov, P.; Yoon, K.B. Capture of iodine and organic iodides using silica zeolites and the semiconductor behaviour of iodine in a silica zeolite. *Energy Environ. Sci.* **2016**, *9*, 1050–1062. [[CrossRef](#)]
21. Chapman, K.W.; Chupas, P.J.; Nenoff, T.M. Radioactive iodine capture in silver-containing mordenites through nanoscale silver iodide formation. *J. Am. Chem. Soc.* **2010**, *132*, 8897–8899. [[CrossRef](#)]
22. Reda, A.T.; Zhang, D.X.; Xu, X.Y.; Xu, S.Y. Highly stable iodine capture by pillared montmorillonite functionalized Bi₂O₃@g-C₃N₄ nanosheets. *Sep. Purif. Technol.* **2022**, *292*, 120994. [[CrossRef](#)]
23. Deuber, H. Investigations on the retention of elemental radioiodine by activated carbons at high temperatures. *Nucl. Technol.* **2017**, *72*, 44–48. [[CrossRef](#)]
24. Zhang, Y.B.; Cui, X.L.; Xing, H.B. Recent advances in the capture and abatement of toxic gases and vapors by metal–organic frameworks. *Mater. Chem. Front.* **2021**, *5*, 5970–6013. [[CrossRef](#)]
25. Mondal, S.; Dastidar, P. Mixed ligand coordination polymers for metallogelation and iodine adsorption. *Cryst. Growth Des.* **2019**, *19*, 470–478. [[CrossRef](#)]
26. Song, S.N.; Shi, Y.; Liu, N.; Liu, F.Q. Theoretical screening and experimental synthesis of ultrahigh-iodine capture covalent organic frameworks. *ACS Appl. Mater. Interfaces* **2021**, *13*, 10513–10523. [[CrossRef](#)]
27. Wang, C.; Wang, Y.; Ge, R.; Song, X.D.; Xing, X.Q.; Jiang, Q.K.; Lu, H.; Hao, C.; Guo, X.W.; Gao, Y.N.; et al. A 3D covalent organic framework with exceptionally high iodine capture capability. *Chem. Eur. J.* **2018**, *24*, 585–589. [[CrossRef](#)]
28. Yin, Z.-J.; Xu, S.-Q.; Zhan, T.-G.; Qi, Q.-Y.; Wu, Z.-Q.; Zhao, X. Ultrahigh volatile iodine uptake by hollow microspheres formed from a heteropore covalent organic framework. *Chem. Commun.* **2017**, *53*, 7266–7269. [[CrossRef](#)]
29. Yan, X.; Yang, Y.X.; Li, G.R.; Zhang, J.H.; He, Y.; Wang, R.; Lin, Z.; Cai, Z.W. Thiophene-based covalent organic frameworks for highly efficient iodine capture. *Chin. Chem. Lett.* **2023**, *34*, 107201. [[CrossRef](#)]
30. Zaguzin, A.S.; Sukhikh, T.S.; Kolesov, B.A.; Sokolov, M.N.; Fedin, V.P.; Adonin, S.A. Iodinated vs non-iodinated: Comparison of sorption selectivity by [Zn₂(bdc)₂dabco]_n and superstructural 2-iodoterephthalate-based metal–organic framework. *Polyhedron* **2022**, *212*, 115587. [[CrossRef](#)]

31. Zaguzin, A.S.; Mahmoudi, G.; Sukhikh, T.S.; Sakhapov, I.F.; Zherebtsov, D.A.; Zubkov, F.I.; Valchuk, K.S.; Sokolov, M.N.; Fedin, V.P.; Adonin, S.A. 2D and 3D Zn (II) coordination polymers based on 4'-(Thiophen-2-yl)-4,2':6',4''-terpyridine: Structures and features of sorption behavior. *J. Mol. Struct.* **2022**, *1255*, 132459. [[CrossRef](#)]
32. Yadollahi, M.; Hamadi, H.; Nobakht, V. Capture of iodine in solution and vapor phases by newly synthesized and characterized encapsulated Cu₂O nanoparticles into the TMU-17-NH₂ MOF. *J. Hazard. Mater.* **2020**, *399*, 122872. [[CrossRef](#)]
33. Li, H.L.; Cheng, D.S.; Cheng, Z.K.; Li, Z.Y.; Li, P.-Z. Effective iodine adsorption by nitrogen-rich nanoporous covalent organic frameworks. *ACS Appl. Nano Mater.* **2023**, *6*, 1295–1302. [[CrossRef](#)]
34. Hasell, T.; Schmidtman, M.; Cooper, A.I. Molecular doping of porous organic cages. *J. Am. Chem. Soc.* **2011**, *133*, 14920–14923. [[CrossRef](#)]
35. Liu, C.; Li, W.L.; Liu, Y.; Wang, H.L.; Yu, B.Q.; Bao, Z.B.; Jiang, J.Z. Porous organic cages for efficient gas selective separation and iodine capture. *Chem. Eng. J.* **2022**, *428*, 131129. [[CrossRef](#)]
36. Chen, X.Y.; Zhang, T.; Han, Y.N.; Chen, Q.; Li, C.P.; Xue, P.C. Multi-responsive fluorescent switches and iodine capture of porous hydrogen-bonded self-assemblies. *J. Mater. Chem. C.* **2021**, *9*, 9932–9940. [[CrossRef](#)]
37. Li, B.; Wang, B.; Huang, X.Y.; Dai, L.; Cui, L.; Li, J.; Jia, X.S.; Li, C.J. Terphen[n]arenes and quaterphen[n]arenes (n = 3–6): One-pot synthesis, self-assembly into supramolecular gels, and iodine capture. *Angew. Chem. Int. Ed.* **2019**, *131*, 3925–3929. [[CrossRef](#)]
38. Luo, D.; Wang, F.; Liu, C.-H.; Wang, S.-T.; Sun, Y.-Y.; Fang, W.-H.; Zhang, J. Combination of aluminum molecular rings with chemical reduction centers for iodine capture and aggregation. *Inorg. Chem. Front.* **2022**, *9*, 4506–4516. [[CrossRef](#)]
39. Feng, Y.; Zou, M.-Y.; Hu, H.-C.; Li, W.-H.; Cai, S.-L.; Zhang, W.-G.; Zheng, S.-R. Amorphous metal-organic frameworks obtained from a crystalline precursor for the capture of iodine with high capacities. *Chem. Commun.* **2022**, *58*, 5013–5016. [[CrossRef](#)]
40. Luo, D.; He, Y.L.; Tian, J.Y.; Sessler, J.L.; Chi, X.D. Reversible iodine capture by nonporous adaptive crystals of a bipyridine cage. *J. Am. Chem. Soc.* **2022**, *144*, 113–117. [[CrossRef](#)]
41. Jie, K.C.; Zhou, Y.J.; Li, E.E.; Li, Z.T.; Zhao, R.; Huang, F.H. Reversible iodine capture by nonporous pillar[6]arene crystals. *J. Am. Chem. Soc.* **2017**, *139*, 15320–15323. [[CrossRef](#)]
42. Yao, S.Y.; Fang, W.-H.; Sun, Y.Y.; Wang, S.-T.; Zhang, J. Mesoporous assembly of aluminum molecular rings for iodine capture. *J. Am. Chem. Soc.* **2021**, *143*, 2325–2330. [[CrossRef](#)]
43. Li, G.L.; Zhuo, Z.; Wang, B.; Cao, X.L.; Su, H.F.; Wang, W.; Huang, Y.G.; Hong, M.C. Constructing π -stacked supramolecular cage based hierarchical self-assemblies via π – π stacking and hydrogen bonding. *J. Am. Chem. Soc.* **2021**, *143*, 10920–10929. [[CrossRef](#)]
44. Li, S.; Li, G.-L.; Wang, W.; Liu, Y.; Cao, Z.-M.; Cao, X.-L.; Huang, Y.-G. A 2D metal-organic framework interpenetrated by a 2D supramolecular framework assembled by CH/ π interactions. *Inorg. Chem. Commun.* **2021**, *130*, 108705. [[CrossRef](#)]
45. Zhao, Q.; Zhu, L.; Lin, G.H.; Chen, G.Y.; Liu, B.; Zhang, L.; Duan, T.; Lei, J.H. Controllable synthesis of porous Cu-BTC@polymer composite beads for iodine capture. *ACS Appl. Mater. Interfaces* **2019**, *11*, 42635–42645. [[CrossRef](#)]
46. Wang, L.Y.; Li, T.; Dong, X.T.; Pang, M.B.; Xiao, S.T.; Zhang, W. Hiophene-based MOFs for iodine capture: Effect of pore structures and interaction mechanism. *Chem. Eng. J.* **2021**, *425*, 130578. [[CrossRef](#)]
47. Pan, X.W.; Ding, C.H.; Zhang, Z.M.; Ke, H.Z.; Cheng, G. Functional porous organic polymer with high S and N for reversible iodine capture. *Microporous. Mesoporous. Mater.* **2020**, *300*, 110161. [[CrossRef](#)]
48. Mahdi, E.M.; Chaudhuri, A.K.; Tan, J.C. Capture and immobilisation of iodine (I₂) utilising polymer-based ZIF-8 nanocomposite membranes. *Mol. Syst. Des. Eng.* **2016**, *1*, 122–131. [[CrossRef](#)]
49. Kim, H.; Doan, V.D.; Cho, W.J.; Madhav, M.V.; Kim, K.S. Anisotropic charge distribution and anisotropic van der waals radius leading to intriguing anisotropic noncovalent interactions. *Sci. Rep.* **2014**, *4*, 5826. [[CrossRef](#)]
50. Rodionov, V.O.; Presolski, S.I.; Gardinier, S.; Lim, Y.H.; Finn, M.G. Benzimidazole and related ligands for Cu-catalyzed azide-alkyne cycloaddition. *J. Am. Chem. Soc.* **2007**, *129*, 12696–12704. [[CrossRef](#)]
51. Sheldrick, G.M. SHELXTL-integrated space-group and crystal-structure determination. *Acta Crystallogr.* **2015**, *A71*, 3–8.
52. Spek, A.L. Single-crystal structure validation with the program PLATON. *J. Appl. Crystallogr.* **2003**, *36*, 7–13. [[CrossRef](#)]

Disclaimer/Publisher's Note: The statements, opinions and data contained in all publications are solely those of the individual author(s) and contributor(s) and not of MDPI and/or the editor(s). MDPI and/or the editor(s) disclaim responsibility for any injury to people or property resulting from any ideas, methods, instructions or products referred to in the content.